When deep diagenesis in Arctic Ocean sediments compromises manganese-based geochronology

Bjorn Sundby [a,b,*], Pascal Lecroart [c], Pierre Anschutz [c], Sergei Katsev [d], Alfonso Mucci [b]

[a] ISMER, Université du Québec à Rimouski, Rimouski, QC, Canada H4C 3J9
(*bjorn.sundby@mcgill.ca)

[b] GEOTOP and Earth & Planetary Sciences, McGill Univ., Montreal, QC, Canada H3A 0E8
(alfonso.mucci@mcgill.ca)

[c] EPOC, Université de Bordeaux, 33405 Talence, France (pierre.anschutz@u-bordeaux.fr;
pascal.lecroart@u-bordeaux.fr)

[d] Large Lakes Observatory & Department of Physics, University of Minnesota Duluth, MN 55812, USA
(skatsev@d.umn.edu)

*Corresponding author:

Bjorn Sundby
Earth & Planetary Sciences
McGill University
3450 University Street, Montreal (Quebec) Canada H3A 2A7
Phone: 1-514-398 4883
Fax: 1-514-398-4680.
E-mail: bjorn.sundby@mcgill.ca

ABSTRACT

We used a diagenetic model to test the hypothesis that manganese-rich layers in gas hydrate-bearing Arctic Ocean sediments are reliable time markers for interglacial periods. In the model, diagenesis is fuelled by two sources of reactive carbon: particulate organic carbon settling to the sediment surface, and methane diffusing up from deep gas hydrate deposits. The model includes oxidation of organic carbon and soluble reduced manganese by oxygen supplied continuously from an invariant bottom-water oxygen reservoir; reduction of particulate manganese by hydrogen sulfide generated through anaerobic methane oxidation; transport of dissolved oxygen and manganese by diffusion; and advective transport of particulate components by burial. Particulate organic matter and particulate manganese are only supplied to the sediment during interglacials. Sulfate reduction is not modeled explicitly; instead, the effect of anaerobic methane oxidation on Mn reduction is simulated at the lower boundary of the model by prescribing that particulate manganese is reduced there to soluble Mn(II). The soluble reduced Mn then diffuses upward and is oxidatively precipitated to Mn(IV) by downward diffusing oxygen. The upward flux of soluble Mn(II) is thus a function of the rate at which particulate manganese is advected into the Mn-reduction layer at the bottom of the model; it is not synchronous with events at the sediment-water interface. Model runs reveal that, under idealized but realistic conditions for the Arctic Ocean, oxidation of upward-diffusing Mn(II) generates post-depositional manganese enrichments that cannot readily be distinguished from the manganese-rich sediment layers that accumulate during interglacials. This compromises the use of manganese-rich layers as proxies for interglacial periods. In contrast, manganese-rich layers may be used as first-order markers of interglacial periods in sediments where gas hydrates or other forms of reactive carbon are absent.

Keywords: Arctic Ocean, sediments, methane oxidation, manganese remobilization, glacial-interglacial cyclicity, modeling.

1. INTRODUCTION

Poor preservation of microfossil records in Arctic Ocean sediments has spurred the search for alternative proxies for the Quaternary chronology of these sediments (Jacobsson, 2000; and references therein). Manganese-rich interbedded layers, found in numerous long cores recovered from the Central Arctic Ocean (März et al., 2011; Löwemark et al., 2014; Macdonald and Gobeil, 2012) are strong candidates as proxies of interglacial periods. A time scale based on manganese content and sediment color in a core from the Lomonosov Ridge correlates closely with an independent paleomagnetic chronology of the same core, based on Brunhes-age estimates of geomagnetic excursions (Jacobsson, 2000; Löwemark et al., 2008). Recent geochemical work has shown that the manganese-rich layers are also rich in several trace metals as well as in biogenic and ice-rafted carbonate and contain preserved traces of bioturbation (März et al., 2011; Löwemark et al., 2014).

There are few measurements of dissolved manganese in long cores from the Arctic. Dickens et al. (2007) measured manganese in a long core from about 1200 m depth on the Lomonosov Ridge and found increasing concentrations of dissolved Mn in the pore water beginning a few m below the sea floor and reaching maximum values at 20 m depth. In a more detailed study, März et al. (2011) working with a long core from 1200 m depth on the Mendeleev Ridge, found an upward directed gradient of dissolved manganese between 6 and

3 m, suggesting possible overprinting of diagenetically mobilized manganese on existing Mn-rich layers.

A scenario, whereby the fluxes of particulate organic carbon and manganese to the sea floor in the Arctic Ocean varied dramatically during the glacial cycles of the Quaternary is consistent with observations. During glaciations, the absence of primary production virtually shuts off the flux of organic carbon, and the ice cover on the continents slows down the delivery of manganese-rich sedimentary material to the sea floor. During interglacials, primary production is turned on and delivers fresh organic carbon to the sea floor while rivers and the expanded continental shelves deliver terrigenous organic carbon and manganese-bearing particulate matter (Macdonald and Gobeil, 2012). Upon burial, manganese-rich interglacial sediments enter the geological record sandwiched between layers of manganese-poor glacial sediment. If the manganese-rich layers remain intact, they mimic the glaciation-interglaciation cyclicity. Several plausible mechanisms for delivering manganese-rich sediment to the sea floor during interglacials have been proposed (e.g. Macdonald and Gobeil, 2012).

The hypothesis that Mn-rich sediment layers enter the geological record intact rests on the assumption that diagenetic remobilization and redistribution of manganese is fuelled exclusively by organic carbon settling from the water column and that manganese diagenesis stops when this carbon has been consumed. The objective of the present study is to test this hypothesis and verify if manganese-rich layers in deep Arctic Ocean sediments can be used as a proxy for interglacial periods. It is not our intention to reconstruct the past. Specifically, we test this hypothesis for sediments that host gas hydrates. Such sediments are abundant in the Arctic Ocean where vast amounts of methane hydrates are believed to be stored (Buffett and Archer, 2004; Klauda and Sandler, 2005). The actual amounts are uncertain (Milkov, 2004).

2. MODEL DESCRIPTION

2.1 The conceptual model

The choice of diagenetic model for this study was dictated by our objective, which was to test the hypothesis that manganese-rich layers in deep Arctic Ocean sediments can be used as a proxy for interglacial periods. To this end, we chose the simplest possible model that would help us meet this objective and left out reactions that could give a more complete description of diagenesis such as oxidation of Fe(II) and ammonia by oxygen and reduction of Fe(III) by hydrogen sulfide. The sedimenting reactive organic matter is assumed to be mineralized entirely through oxic respiration (the mineralization process is carbon limited), so a more complex model that includes the products of anaerobic mineralization pathways would not be expected to change our conclusions.

The model we used is a one-dimensional non-steady state diagenetic transport-reaction model that captures the essential features of manganese diagenesis, i.e. reduction of Mn(IV) to Mn(II) (dissolution), reoxidation of Mn(II) to Mn(IV) (precipitation), transport of dissolved manganese by diffusion, and transport of precipitated manganese by advection. Figure 1 shows the conceptual version of the model. It includes two sources of reactive organic carbon: fresh organic matter settling through the water column and methane released from gas hydrates deep in the sediment column. The reactive organic carbon deposited on the sediment surface is consumed in reactions with dissolved oxygen as it is buried and advected downward. Oxygen diffuses into the sediment from a permanently oxygenated water column. The second source of carbon, methane, is oxidized by micro-organisms that use sulfate as a terminal electron acceptor. This process, anaerobic methane oxidation (AMO), is known to take place in

119 the sulfate-methane transition layer (SMT) where upward diffusing methane and downward
120 diffusing sulfate are consumed and become depleted. AMO produces sulfide, which reduces
121 oxidized particulate Mn(IV) to soluble Mn(II) (Aller and Rude, 1988). Methane may also reduce
122 oxidized manganese directly (Beal et al., 2009). The model domain is bounded at the top by
123 the sediment surface and at the bottom by a depth that remains at a fixed distance from the
124 upper boundary. Thus, both boundaries move upwards at the rate with which sediment
125 accumulates, set at 1 cm Ky^{-1} in the model. One may reasonably expect that the sediment
126 accumulation rate is higher during interglacials than during glacials and, therefore, that the
127 assumption of constant sedimentation rate may not be realistic. Nonetheless, since the since
128 the differential rates are not known, and given that the spatial scale of Mn redistribution (~2 m)
129 is greater than the thickness of layer of sediment deposited during one cycle, making this
130 assumption is not expected to change the conclusions.
131 The reactions in the SMT that produce hydrogen sulfide are not included explicitly in the
132 model, nor is the reduction of Mn(IV) to Mn(II) by hydrogen sulfide. Instead, reducing
133 conditions are prescribed near the bottom of the model domain. There, particulate oxidized
134 manganea, advected downward by burial, is reduced to soluble Mn(II), which diffuses upwards
135 until reoxidized by downward diffusing oxygen. The thickness of the prescribed reduction layer
136 (a few cm in the numerical model implementation) is not critical because the production rate of
137 dissolved Mn(II) is transport controlled, i.e. the rate of reductive dissolution overwhelms the
138 rate of supply of reducible manganese. The choice of a 5-m thick model domain was inspired
139 by the data of März et al. (2011), which suggest that dissolved manganese is produced at
140 about this depth in their Lomonosov Ridge core.
141 Since the model assumes that the entire sedimentation flux of reactive organic matter is
142 consumed by oxygen, early diagenesis of manganese within the interglacial layer is not

included, nor are fluctuations in the flux of particulate manganese and organic carbon that could create multiple peaks within an interglacial layer (Katsev et al., 2006). Multiple peaks in the manganese content of a layer being advected towards the deep reduction zone will affect the instantaneous production rate of soluble reduced manganese in the reduction zone, but it will not change the total dissolved-manganese flux originating in that layer.

The oxygen flux and the penetration of oxygen into the sediment are governed by the oxidation of organic carbon and reduced manganese. At the end of an interglacial, the manganese-rich layer is covered by sediment free of organic carbon and manganese and is progressively buried. Consequently, oxygen diffuses further down into the sediment as it progressively oxidizes the reactive organic carbon that was supplied and survived oxidation during the interglacial period.

The choice to keep the lower boundary of the model domain at a fixed distance from the sediment surface throughout a glacial cycle was pragmatic considering the complexity of the processes that act upon the depth of the SMT. On the one hand, interrupting the flux of organic carbon to the sediment at the end of an interglacial period would deepen the oxygen penetration and the depth of the SMT (Contreras et al., 2013). On the other hand, the lowering of the sea level that characterizes a glacial period decreases the pressure on the sediment and causes the stability field of gas hydrates, and thus the depth at which gas hydrates decompose and release methane, to move closer to the sediment surface (Dickens, 1995; Paull et al., 1999). The combined effect of these two opposing processes on the location within the sediment of the SMT would be difficult to predict, but we will attempt to addres it in a subsequent paper.

2.2 Numerical implementation

167 The conceptual model was implemented numerically as a transient transport-reaction
168 model (e.g. Donnadieu et al., 2002; Berg et al., 2003), the details of which are described in
169 Table 1. As outlined above, the model complexity was limited to the processes and species
170 that relate to manganese diagenesis on the time scale considered. The parameter values we
171 used are listed in Table 2. Dissolved species are Mn(II) and O_2. Solid species are manganese
172 oxide (Mn(IV)) and labile organic carbon (OC). Particulate OC is deposited by sedimentation at
173 the top of the domain.
174 As described above, the flux of particulate manganese to the sediment was kept
175 constant during the interglacial period and was null during the glacials. The abrupt transition in
176 the manganese flux at the beginning and the end of an interglacial period could cause
177 numerical problems for the model. To smoothen the transitions at the beginning and end of an
178 interglacial and thus avoid this problem, we included particle mixing in the 6 cm thick surface
179 layer. The particle mixing was modeled as a diffusion analogous process, equivalent to
180 biodiffusion. The mixing coefficient was kept constant from 0-3 cm, below which it decayed
181 exponentially to zero at 6 cm (e.g. Maire et al., 2008). The mixing process generates a layer of
182 manganese-rich sediment in which the vertical manganese distribution has the shape of a
183 Gaussian curve. This layer is then buried.
184 Diffusion affects the distribution of soluble species and is described in porous media by
185 Fick's first law with their respective diffusivities corrected for tortuosity. Porosity is assumed
186 constant, a fair assumption below a few tens of centimeters. Burial is assumed to be an
187 advective process with constant burial velocity. The concentration of oxygen is assumed
188 constant at the upper boundary and zero at the lower boundary. A zero dissolved manganese
189 concentration is imposed at the top of the model domain, and a zero flux of dissolved Mn is
190 imposed at the base of the domain. Imposing a zero Mn(II) flux across the lower model

boundary ignores the possible presence of sink for Mn(II) deeper in the sediment such as the coprecipitation of Mn(II) with calcium carbonate or the precipitation of a distinct Mn(II) carbonate. We have no information that can be used to establish the location of such a sink (depth below the lower model boundary) and can therefore not estimate a downward directed gradient and flux of Mn(II). In the absence of a flux across the lower boundary, the inventory of manganese within the model domain builds up, and eventually—over several glacial-interglacial cycles—leads to a shallowing of the oxygen penetration depth during interglacials (see fig. 3).

We applied a repeating pattern of high fluxes of OC and Mn(IV) during interglacials and null fluxes of OC and Mn(IV) during glacials (Table 1). The model was tuned by varying the flux and the reactivity of the OC and the duration of the interglacial period until the model produced manganese oxide profiles comparable to profiles not subjected to diagenesis. The equations for conservation of mass for the four species were solved using a finite element approach implemented with the PDE module of COMSOL Multiphysics ®.

3. RESULTS AND DISCUSSION

3.1 Burial of manganese-rich layers in sediments where gas hydrates are absent

In the absence of decomposing gas hydrates that can supply methane to the sediment pore water, the Mn-rich interglacial sediment layers would remain intact once buried. Under these conditions, the model does not falsify the hypothesis that manganese-rich layers in Arctic Ocean sediments can be used as a proxy for interglacial periods. Although this statement is self-evident, it is not trivial, because it offers the means to locate a sedimentary manganese record that has not been compromised by post-depositional alterations. As pointed out by

215 Borowski et al. (1996,1999), the pore-water sulfate distribution is sensitive to the presence of
216 sub-surface methane and, thus, the absence of a sulfate gradient can be interpreted as an
217 absence of decomposing gas hydrates.
218
219 ***3.2 Burial of manganese-rich layers in gas hydrate containing sediments*** .
220 Reducing conditions generated by the presence of methane at depth in the sediment
221 column lead to the remobilization and redistribution of manganese. Figure 2 illustrates this with
222 a model run over five successive glacial-interglacial cycles, each lasting 100 Ky. During the
223 interglacial period of each cycle, manganese was added to the sea floor, where sediment
224 accumulation and particle mixing combined to generate a Gaussian-shaped peak in the vertical
225 manganese distribution. When the run started, the 5-m thick sediment column contained five of
226 these layers, identical and equally spaced as the initial condition for the Mn(IV) distribution.
227 During the run, 5 m of new sediment – including five new manganese-rich layers – were added
228 to the sediment column while the top of the model domain kept track with the upward moving
229 sea floor. By the end of the model run, the initial five interglacial layers had been advected into
230 the reduction layer (SMT), and their manganese content had been remobilized and
231 redistributed in the overlying sediment column. Of the five interglacial layers added to the
232 sediment column during the course of the model run, the two most recent ones were not
233 altered, but the three older layers grew in size and changed shape because of the precipitation
234 of remobilized manganese.
235 Figure 2 demonstrates that even when one starts out with a simple pattern of solid-
236 phase manganese distributed across the sediment column, the distribution pattern that results
237 from diagenesis can be complex. In this model run, most of the remobilized manganese is
238 redistributed across the deeper part of the sediment column; none of it seems to reach above

about 2 m below the sediment surface. This result can be understood in light of the cyclic pattern of the oxygen penetration into the sediment. Figure 3 shows that during most of this run, oxygen penetrates nearly to the bottom of the model domain. Only during (relatively) brief periods of time does the penetration depth rise towards the upper reaches of the sediment column. The timing of the shallow oxygen penetration events coincides with the interglacial part of the cycle, as could be expected since this is when fresh reactive organic carbon is delivered to the sea floor. It follows that this is the time when dissolved manganese – if present in the pore water – can be transported closest to the sea floor before being oxidized and reprecipitated. The relatively deep oxygen penetration in the model results during these periods can be attributed to the relatively low value we used for the organic carbon flux to the sediment during the interglacials.

The complexity of the diagenetic remobilization of manganese is further illustrated in figure 4, which shows the results of a model run over a single glacial cycle, beginning when the bottom of a thick manganese-rich layer enters the reduction zone at the bottom of our sediment column. At the end of the 50 Ky cycle, the deepest Mn-rich layer (400-500 cm) had been reductively dissolved. The layer at 350 cm depth had been buried and grown in intensity because of the increased background concentration of Mn(IV). A new Mn-rich layer had appeared at 200-250 cm, and the original Mn-rich layer at 50 cm had been buried intact. Faced with the complexities of manganese diagenesis in our simple model sediment, it cannot be assumed that manganese-rich layers found in gas hydrate bearing sediments are primary features, laid down during interglacial periods.

3.3 The deep manganese cycle

The presence and distribution of dissolved manganese in the pore water depend on the advection of manganese-rich sediment across the upper boundary of the reduction zone (SMT), the timing of which is unlikely to be synchronous with the oxygen penetration pattern. Most of the time, as shown in figure 3, oxygen is present deep in the sediment, close to the bottom of the model domain. Therefore, the conditions in the pore water will be oxidizing most of the time and any dissolved manganese produced will only be able to diffuse a short distance before it is oxidized and precipitated. Except during and shortly after interglacial periods when oxygen penetration is shallow, dissolved manganese will reprecipitate deep in the sediment, close to the SMT, and oxidized Mn may accumulate, perhaps to high levels, before it is buried again and enters a new cycle of dissolution, diffusion, oxidation, and burial. The deep recycling of manganese, the results of which can be seen just above the dissolution zone in figure 2, explains why the redistribution pattern of manganese is decoupled from the distribution pattern in the sediment column that undergoes burial.

4. Conclusion

A one-dimensional non-steady state diagenetic transport-reaction model reveals that destabilization of deep-seated gas hydrates and subsequent oxidation via anaerobic sulfate oxidation of methane diffusing up in the sediment column may remobilize manganese-rich sediment layers and thus compromise the use of such layers in Arctic Ocean sediments as a primary record of glacial-interglacial transitions. Unfortunately, neither the redistribution of manganese-rich layers nor the original manganese record can be readily reconstructed because vertical excursions of the sediment oxygen penetration depth (temporal variations in the distribution of dissolved oxygen in the sediment column) and the production of dissolved

Mn (burial of manganese-rich layers in the sulfate methane transition zone) are not likely to be in phase.

In contrast, where methane or other forms of secondary organic matter are absent from sediments, manganese-rich layers deposited during interglacials will be preserved, and their presence in the sediment column can be used as a proxy of interglacial periods. The absence of a sulfate gradient in the sediment pore-water is an indicator of this type of sediment because the sulfate distribution is sensitive to the presence of sub-surface methane.

Acknowledgements

The work of Dr. Christian März and his colleagues inspired this study, and Dr. März gave us access to their geochemical data from the Arctic Ocean. Comments and suggestions by Dr. David Burdige and an anonymous reviewer helped improve the manuscript. The Canadian Natural Research and Engineering Council and the Université de Bordeaux provided financial support. Bacchus, the God of Wine, provided spiritual guidance. We thank them all.

References

Aller, R.C., Rude, P.D., 1988. Complete Oxidation of Solid-Phase Sulfides by Manganese and Bacteria in Anoxic Marine-Sediments. Geochimica et Cosmochimica Acta, 52(3): 751-765.

Beal, E.J., House, C.H., Orphan, V.J., 2009. Manganese- and Iron-Dependent Marine Methane Oxidation. Science, 325(5937): 184-187.

Berg, P., Rysgaard, S., Thamdrup, B., 2003. Dynamic modeling of early diagenesis and nutrient cycling. A case study in an Arctic marine sediment. American Journal of Science, 303(10): 905-955.

Borowski, W.S., Paull, C.K., Ussler, W., 1996. Marine pore-water sulfate profiles indicate in situ methane flux from underlying gas hydrate. Geology, 24(7): 655-658.

310 Borowski, W.S., Paull, C.K., Ussler, W., 1999. Global and local variations of interstitial sulfate gradients
311 in deep-water, continental margin sediments: Sensitivity to underlying methane and gas
312 hydrates. Marine Geology, 159(1-4): 131-154.
313 Boudreau, B.P., 1997. Diagenetic models and their implementation: modelling, transport and reactions
314 in aquatic sediments. Springer Verlag, Berlin.
315 Buffett, B., Archer, D., 2004. Global inventory of methane clathrate: sensitivity to changes in the deep
316 ocean. Earth and Planetary Science Letters, 227(3-4): 185-199.
317 Clough, L.M., Ambrose, W. G., Cochran, J. K., Barnes, C., Renaud, P. E., Aller, R. C., 1997. Infaunal
318 density, biomass and bioturbation in the sediments of the Arctic Ocean. Deep-Sea Research II,
319 44: 1693-1704.
320 Contreras, S., Meister, P., Liu, B., Prieto-Mollar, X., Hinrichs, K. U., Khalili, A., Ferdelman T.G., Kuypers
321 M.M.M., Jørgensen, B. B. (2013)). Cyclic 100-ka (glacial-interglacial) migration of subseafloor
322 redox zonation on the Peruvian shelf. *Proceedings of the National Academy of Sciences*,
323 *110*(45), 18098-18103.
324 Dickens, G. R., Koelling, M., Smith, D. C., & Schnieders, L. (2007). Rhizon sampling of pore waters on
325 scientific drilling expeditions: an example from the IODP Expedition 302, Arctic Coring
326 Expedition (ACEX). *Scientific Drilling*, *4*(4), 1-4.
327 Dickens, G.R., O'Neill, J.R., Rea, D.R., Owen, R.M. 1995. Dissociation of oceanic methane hydrate as
328 a cause of the carbon isotope excursion at the end of the Paleocene. Paleoceanography, 10(6):
329 965-971.
330 Donnadieu, Y., Lecroart, P., Anschutz, P., Bertrand, P., 2002. Bias in the paleoceanographic time
331 series: Tests with a numerical model of U, C-org, and Al burial. Paleoceanography, 17(3):
332 10.1029/2001PA000638
333 Jacobsson, M., Løvlie, R., Al-Hanbali, H., Arnold, E., Backman, J.Morth, N., 2000. Manganese and
334 color cycles in Arctic Ocean sediments constrain Pleistocene chronology. Geology, 28(1): 23-26.

Katsev, S., Sundby, B., Mucci, A., 2006. Modeling vertical excursions of the redox boundary in sediments: Application to deep basins of the Arctic Ocean. Limnology and Oceanography, 51(4): 1581-1593.

Klauda, J.B., Sandler, S.I., 2005. Global distribution of methane hydrate in ocean sediment. Energy & Fuels, 19(2): 459-470.

Löwemark, L., Jakobsson, M., Morth, M., Backman, J., 2008. Arctic Ocean manganese contents and sediment colour cycles. Polar Research, 27(2): 105-113.

Löwemark, L., März , C., O'Regan, M., Gyllencreutz, R., 2014. Arctic Ocean Mn-stratigraphy: genesis, synthesis and inter-basin correlation. Quaternary Science Reviews, 92: 97-111.

Macdonald, R.W., Gobeil, C., 2012. Manganese Sources and Sinks in the Arctic Ocean with Reference to Periodic Enrichments in Basin Sediments. Aquatic Geochemistry, 18(6): 565-591.

Maire, O. Lecroart P., Meysman F.J.R., Rosenberg R., Duchene J.C., Grémare A., 2008.. Quantification of sediment reworking rates in bioturbation research: a review. Aquatic Biology, 2(3): 219-238.

März, C., Stratmann, A., Matthiessen, J., Meinhardt, A.-K., Eckert, S., Schnetger, B., Vogt, C., Brumsack, H.-J, 2011. Manganese-rich brown layers in Arctic Ocean sediments: Composition, formation mechanisms, and diagenetic overprint. Geochimica et Cosmochimica Acta, 75(23): 7668-7687.

Milkov, A.V., 2004. Global estimates of hydrate-bound gas in marine sediments: how much is really out there? Earth-Science Reviews, 66(3-4): 183-197.

Paull, C.K., Ussler, W., Dillon, W.P., 1991. Is the Extent of Glaciation Limited by Marine Gas-Hydrates. Geophysical Research Letters, 18(3): 432-434.

Figure legends

Figure 1. Spatial representation of the conceptual model. In the time evolution of this system, the processes associated with step 4 only take place once step 5 has occurred for the first time.

Figure 2. Distribution of oxidized particulate manganese (upper panels), reduced dissolved manganese (middle panels), and dissolved oxygen (lower panels) in a model sediment at the beginning and during a run of five successive glacial-interglacial cycles. Each cycle lasted 100 ka. During each interglacial period, particulate manganese was added at the sediment surface, generating a Gaussian-shaped solid-phase manganese peak. In the absence of reducing conditions at the bottom of the model domain, these peaks would remain intact, leading to the pattern of equally-spaced identically-shaped manganese peaks propagating downward. This distribution was then used as the initial state for a run of five glacial cycles, during which reducing conditions were imposed at the bottom of the model domain. The resulting pattern (t = 500 ka) shows that new manganese-rich layers appeared below 175 cm sub-bottom depth. The background concentration and the inventory of manganese increased, but the increase is restricted to depths below 175 cm. Panels at t= 125 ka and t = 140 ka show two contrasting situations during glacial and interglacial intervals, respectively.

Figure 3: Model calculations of the temporal variations of the oxygen penetration depth into the sediment (in meters below sea floor). The shallowest oxygen penetration occurs during the interglacials. After an interglacial, oxygen penetration increases rapidly as it burns through residual reactive OC and remains deep until the beginning of a new interglacial when the delivery of reactive OC to the sea floor rapidly draws it back closer to the surface (Katsev et al., 2006). Dissolved manganese, originating in the deepest model domain, precipitates when it encounters oxygen and, thus, the depth where dissolved manganese reprecipitates tracks the oxygen penetration depth. The actual upward flux of dissolved manganese is determined by the advection of manganese-rich sediment into the manganese reduction zone (SMT) at the bottom of the model domain. The gradual shallowing of the oxygen penetration depth with time in the model calculation reflects the progressive accumulation of manganese within the model domain, a consequence of imposing zero flux of dissolved Mn(II) at the lower model boundary.

393

394 **Figure 4**: Distribution of oxidized particulate manganese (upper panels), reduced dissolved
395 manganese (middle panels), and dissolved oxygen (lower panels) of manganese-rich
396 sediment after a single glacial-interglacial cycle. The initial solid-phase manganese distribution
397 (upper right panel) consisted of three different manganese-rich layers un-equally spaced over
398 a 5-m sediment column. Note the erosion of the deepest manganese-rich layer, the
399 appearance of a new manganese-rich layer beginning at 2 m depth, and the increase in the
400 background concentration of oxidized manganese below 2 m depth. Note also the shift in the
401 oxygen penetration depth due to the presence/absence of a layer, rich in Mn and organic
402 carbon, at the surface.

403

404

Table 1. Model description

Dissolved and solid species included in the model

	Species	Variable	Unit
Solutes	Oxygen	O_2	mmol/cm^3
	Manganese	Mn^{2+}	mmol/cm^3
Solids	Organic matter	OC	mmol/cm^3
	Manganese oxide	MnOx	mmol/cm^3

Primary and secondary redox reactions

$OC = CH_2O$

$OC + O_2 \longrightarrow \Sigma CO_2 + H_2O$ (R_{OM})

$2\ Mn^{2+} + O_2 + 4\ HCO_3^- \longrightarrow 2\ MnO_2 + 4\ CO_2 + 2\ H_2O$ (R_1)

Near the bottom of the model domain, it is assumed that a reductant is present in sufficient concentration to completely reduce the MnO_x that reaches this boundary

MnO_x + reductant $\longrightarrow Mn^{2+}$ (R_2)

Mass conservation equations

$$\frac{\partial \varepsilon C_i}{\partial t} = \frac{\partial}{\partial z}\left(\varepsilon \mathrm{D_i}' \frac{\partial C_i}{\partial z}\right) - \frac{\partial}{\partial z}(\varepsilon \mathrm{w} C_i) + \sum_j \varepsilon R_j$$

t = time (ka);

z = vertical coordinate (positive downwards, cm);

C_i = solid or solute concentration (mmol/cm^3);

$\varepsilon = \varphi$ for solute species and $(1-\varphi)$ for solid species;

φ = porosity; φ is constant with depth;

for solutes, D'_i = effective diffusion coefficient, corrected for tortuosity;

for solids, D'_i = Db = particle mixing coefficient (cm^2/ka)

w = sedimentation rate (cm/ka); w is assumed constant with time.

R_j = rates of chemical reactions (mmol/cm^3/ka) for the different species:

$R_{OM} = -\ k\ OC$

$R_{Ox} = -\ F\ k\ OC - R_1$ with F being the conversion factor, $F = (1 - \varphi) / \varphi$

$R_{Mn} = -2\ R_1 + F\ R_2$

$R_{MnOx} = -\ R_2 + (2/F)\ R_1$

$R_1 = k_{1MnOx}\ O_2\ Mn^{2+}$

$R_2 = k_{2MnOx}\ MnO_x$

Boundary conditions

	OC	O_2	Mn^{2+}	*MnOx*
z_0	$F_{OM\ inter\ z0} \times \Omega(t)$	$O_{2\ z0}$	$Mn^{2+}_{\ z0}$	$F_{MnOx\ inter\ z0} \times \Omega(t)$
z_b	no gradient	$O_{2\ zb}$	$F_{Mn\ zb}$	no gradient

$\Omega(t)$ is the time function

Initial conditions

At t = 0,

$OC(z)$ = 0 mmol/cm^3

$Mn^{2+}(z)$ = 0 mmol/cm^3

$MnO_x(z)$ = $MnO_{x\text{-inter}}$ $\chi(z)$

$O_2(z)$ = 0 mmol/cm^3

For instance on Figure 2, $\chi(z)$ is defined by

$$\chi(z) = \sum_{i=1}^{m}\left(\frac{1}{1+\exp\left(-\left(x-x_i\right)/\tau\right)} + \frac{1}{1+\exp\left(\left(x-x_i^{'}\right)/\tau\right)}\right) - m$$

x_i = 40 + 100 (i-1)

x_i' = 60 + 100 (i-1)

τ is a constant

m = number of initial peaks (m = 5)

Time functions

$$F(t) = F_{glac} + \left(F_{inter} - F_{glac}\right) \times \Omega(t)$$

with F = $F_{OM\ z0}$ or $F_{MnOx\ z0}$

$$\Omega(t) = \sum_{i=1}^{n}\left(\frac{1}{1+\exp\left(-\left(t-t_i\right)/\tau\right)} + \frac{1}{1+\exp\left(\left(t-t_i^{'}\right)/\tau\right)}\right) - n$$

with

$$t_i = \left(t_{glac} + t_{inter}\right) \times i - t_{inter}$$

$$t_i^{'} = \left(t_{glac} + t_{inter}\right) \times i$$

n is the number of glacial-interglacial cycles during the simulation (n = 5)

τ is a constant

Table 2. Model input parameters

Parameter	Value	Cited values	Sources
Top of the calculation domain	z_0 = 0 cm		
Bottom of the domain	z_b = 1000 (500 ?) cm		
Temperature	T= 2°C		1
Porosity	φ= 0.6		1
Time parameters	t_{inter} = 20 ka		
	t_{glac} = 80 ka		
	τ = 1.5 ka		
	n = 5		
Simulation time	Γ = 1000 ka		
Sedimentation rate	w = 1 cm/ka	0.1 - 1	1, 2
Diffusion coefficients	$D_{O2} = 44.10^4$ cm^2/ka		3
	$D_{Mn} = 11.10^4$ cm^2/ka		3
Tortuosity	$\theta = \varphi^{1.14}$		1
Particle mixing coefficient	Db = 70 cm^2/ka	40 - 100	1, 2
	η = 0.5 cm		
Mixing layer depth	L = 3 cm	2 – 5	1, 2
Boundary conditions for solutes	$O_{2\ z0} = 2.10^{-4}$ mmol/cm^3		1
	$Mn^{2+}_{\ z0}$ = 0 mmol/cm^3		
	$O_{2\ zb}$ = 0 mmol/cm^3		
	$F_{Mn\ zb}$ = 0 mmol/cm^2/ka		
Boundary conditions for solids	$F_{OM\ inter\ z0}$ = 150 mmol/cm^2/ka	8 - 100	1
	$F_{OM\ glac\ z0}$ = 0 mmol/cm^2/ka		
	$F_{MnOx\text{-}inter\ z0}$ = 0.1 mmol/cm^2/ka		
	$F_{MnOx\ glac\ z0}$ = 0 mmol/cm^2/ka		
	$(\partial MnOx/\partial z)_{z_b} = 0$		1
Initial condition	$MnOx_{inter}$= 0.24 mmol/cm^3	0.04 0.24	
	m	5	
Rate constant	k = 10 ka^{-1}	4 10^{-2} - 100	1
	$k_{1MnOx} = 142.10^7$ cm^3/mmol/ka	$(35 – 250)10^7$	1, 5
	k_{2MnOx} = 60 ka^{-1}	0 - 60	5

1. (Katsev et al., 2006); 2. (Clough, 1997); 3. (Boudreau, 1997); 4. (Marz et al., 2011); 5. (Berg et al., 2003)

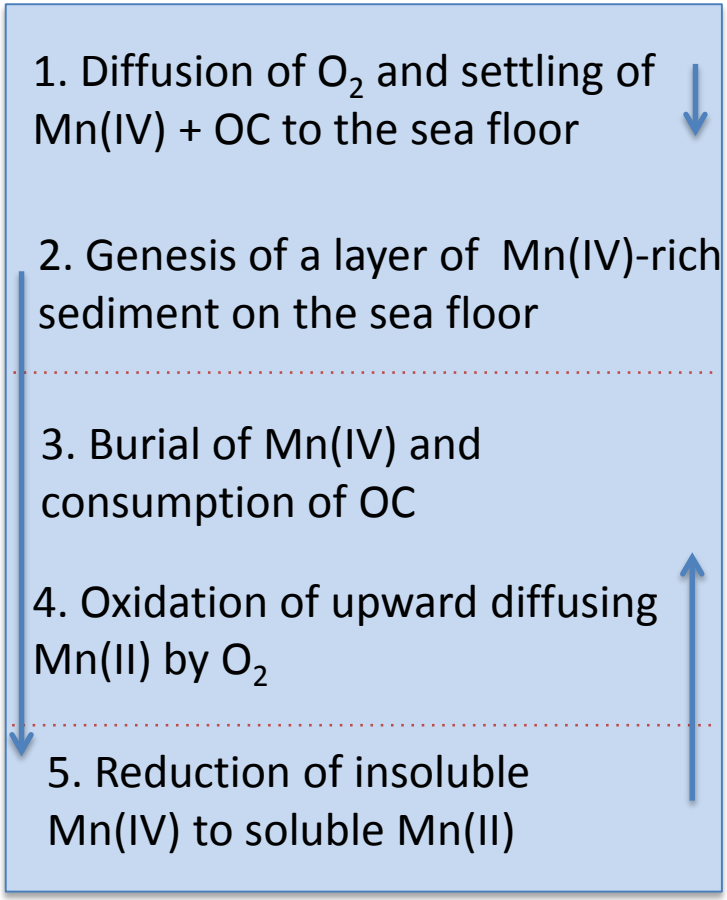

① Bottom water [O_2] is constant; settling fluxes of Mn(IV) and OC are constant during interglacials and zero during glacials.

② Accumulation of Mn(IV)-rich settling particulate matter through the water column forms a Mn(IV)-rich layer on the sea floor

③ During burial, OC becomes exhausted and the Mn(IV)-rich layer generated during an interglacial is preserved until it reaches the reduction zone.

④ Mn(II) is reoxidized and precipitated as Mn(IV) when it encounters downward diffusing O_2. The O_2 penetration depth depends on the oxygen demand of OM and Mn(II) oxidation.

⑤ Anaerobic methane oxidation creates a reducing environment where insoluble Mn(IV) is reduced to soluble Mn(II). The upward flux of Mn(II) from this layer equals the flux of Mn(IV) into the layer. The fluxes depend on the distribution of Mn(IV) in the sediment column and the burial rate.

Figure 1. Spatial representation of the conceptual model. In the time evolution of this system, the processes associated with step 4 only take place once step 5 has occurred for the first time.

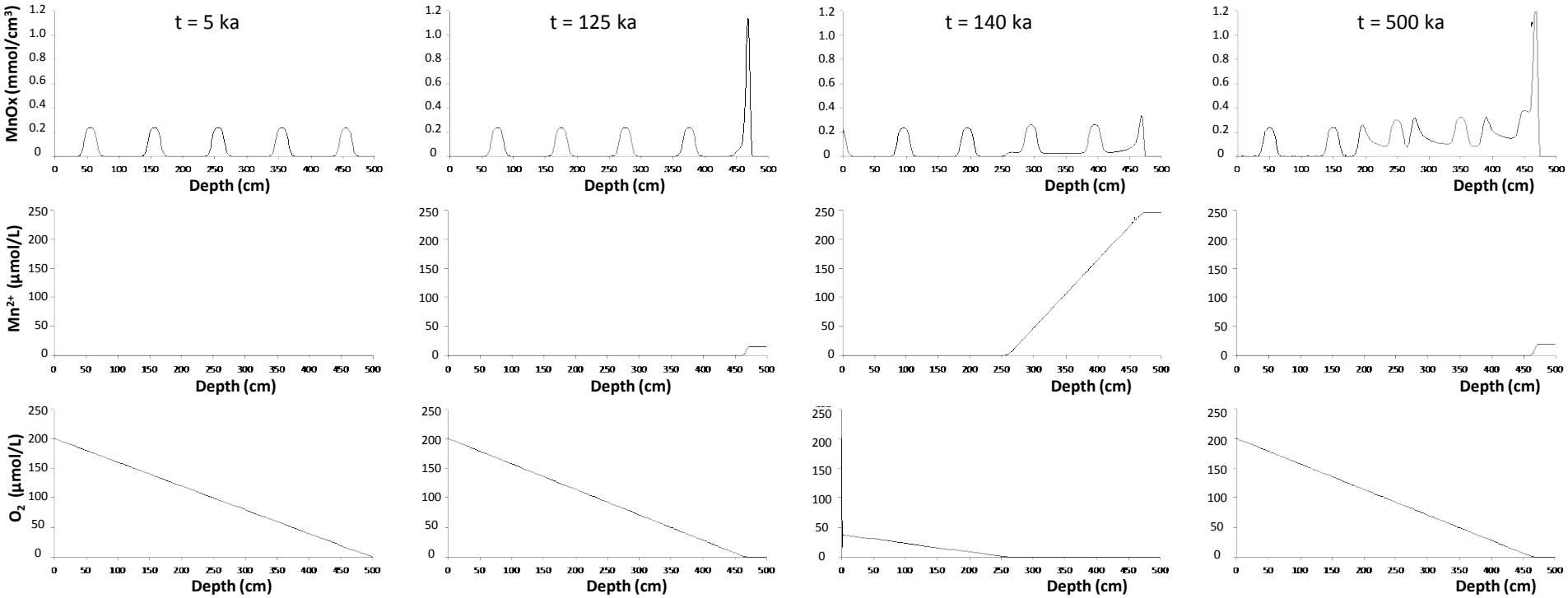

Figure 2. Distribution of oxidized particulate manganese (upper panels), reduced dissolved manganese (middle panels), and dissolved oxygen (lower panels) in a model sediment at the beginning and during a run of five successive glacial-interglacial cycles. Each cycle lasted 100 ka. During each interglacial period, particulate manganese was added at the sediment surface, generating a Gaussian-shaped solid-phase manganese peak. In the absence of reducing conditions at the bottom of the model domain, these peaks would remain intact, leading to the pattern of equally-spaced identically-shaped manganese peaks propagating downward. This distribution was then used as the initial state for a run of five glacial cycles, during which reducing conditions were imposed at the bottom of the model domain. The resulting pattern (t = 500 ka) shows that new manganese-rich layers appeared below 175 cm sub-bottom depth. The background concentration and the inventory of manganese increased, but the increase is restricted to depths below 175 cm. Panels at t= 125 ka and t = 140 ka show two contrasting situations during glacial and interglacial intervals, respectively.

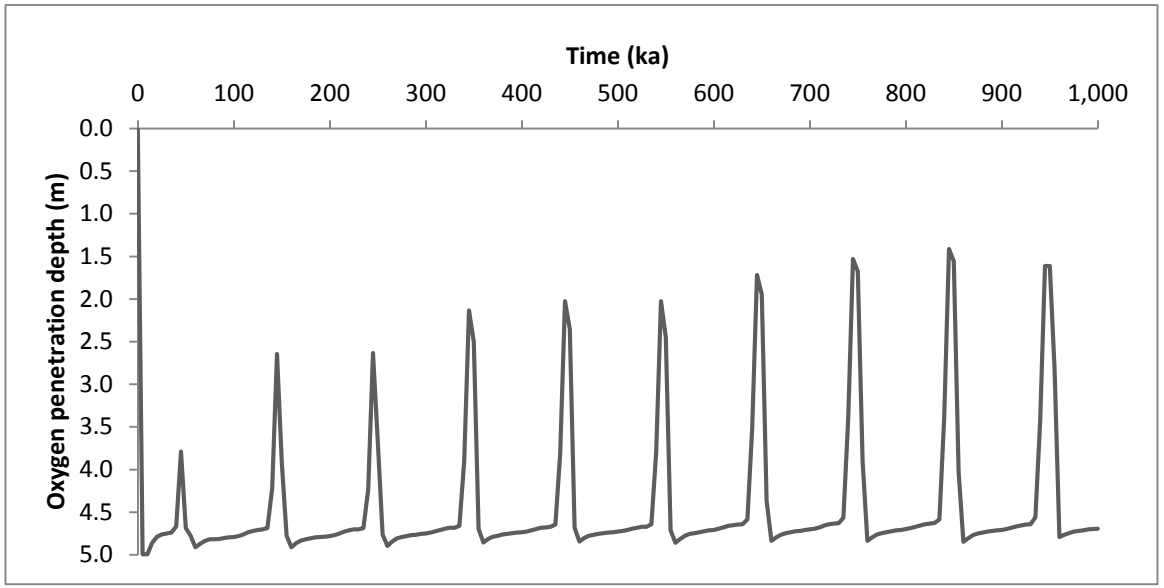

Figure 3: Model calculations of the temporal variations of the oxygen penetration depth into the sediment (in meters below sea floor). The shallowest oxygen penetration occurs during the interglacials. After an interglacial, oxygen penetration increases rapidly as it burns through residual reactive OC and remains deep until the beginning of a new interglacial when the delivery of reactive OC to the sea floor rapidly draws it back closer to the surface (Katsev et al., 2006). Dissolved manganese, originating in the deepest model domain, precipitates when it encounters oxygen and, thus, the depth where dissolved manganese reprecipitates tracks the oxygen penetration depth. The actual upward flux of dissolved manganese is determined by the advection of manganese-rich sediment into the manganese reduction zone (SMT) at the bottom of the model domain. The gradual shallowing of the oxygen penetration depth with time in the model calculation reflects the progressive accumulation of manganese within the model domain, a consequence of imposing zero flux of dissolved Mn(II) at the lower model boundary.

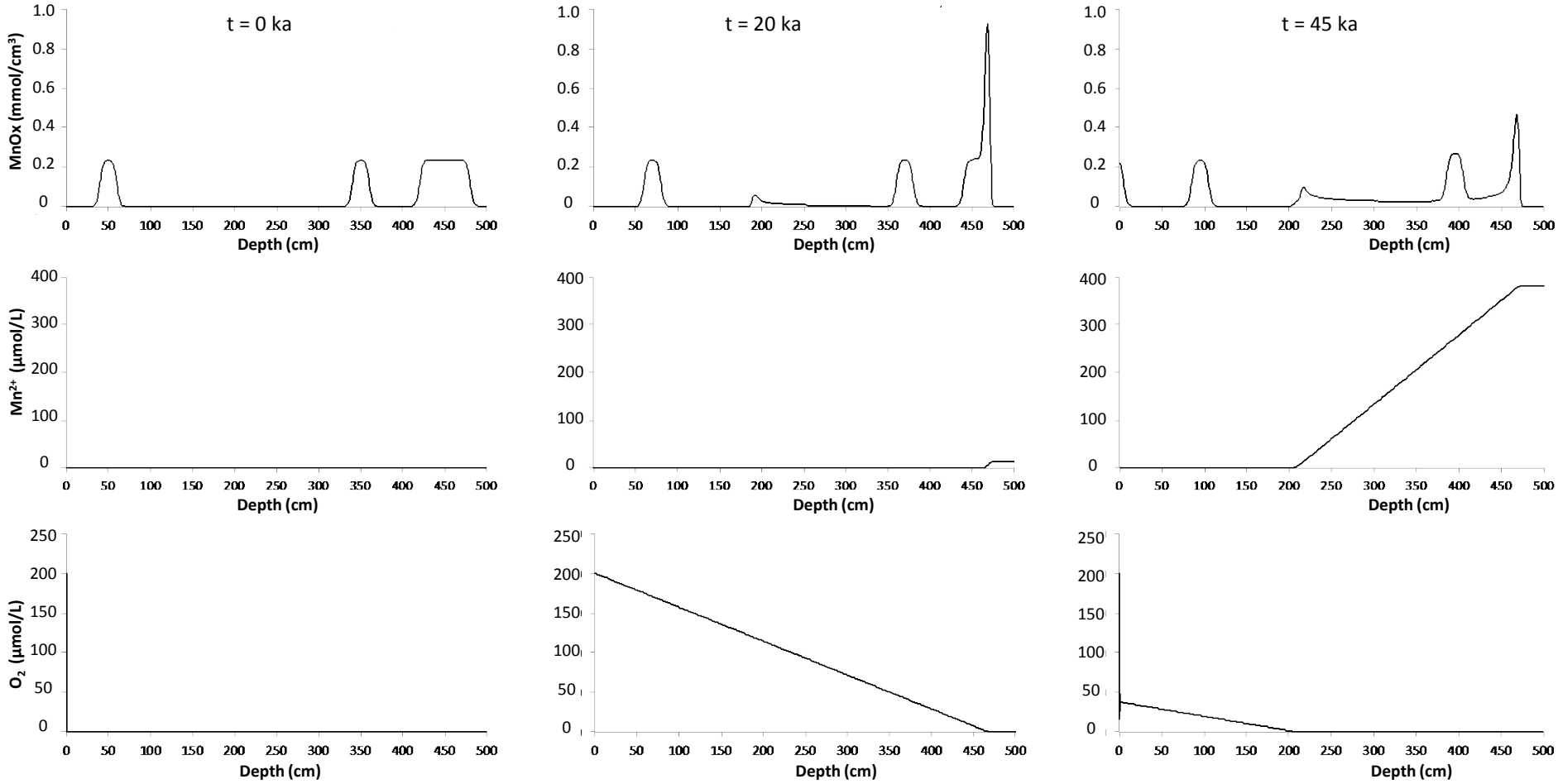

Figure 4: Distribution of oxidized particulate manganese (upper panels), reduced dissolved manganese (middle panels), and dissolved oxygen (lower panels) of manganese-rich sediment after a single glacial-interglacial cycle. The initial solid-phase manganese distribution (upper right panel) consisted of three different manganese-rich layers un-equally spaced over a 5-m sediment column. Note the erosion of the deepest manganese-rich layer, the appearance of a new manganese-rich layer beginning at 2 m depth, and the increase in the background concentration of oxidized manganese below 2 m depth. Note also the shift in the oxygen penetration depth due to the presence/absence of a layer, rich in Mn and organic carbon, at the surface.